Eurasian Journal of Physics and Functional Materials

2026, 10(2), 164-177

Digital technology for growing alkali halide crystals in an argon atmosphere based on the Bridgman method

K.Sh. Shunkeyev, Sh. Sagimbayeva*, A. Kenzhebayeva, Zh. Ubaev*

K. Zhubanov Aktobe Regional University, Aktobe, Kazakhstan

E-mail: sh.zh.sagimbaeva@gmail.com, zubaev@zhubanov.edu.kz

DOI: **10.32523/ejpfm.2026100205**
Received: 20.04.2026 - after revision

A process for the purification and growth of alkali halide crystals (AHCs) has been demonstrated using the KCl:Li crystal as a representative example. The experiments were performed on an experimental crystal growth setup manufactured by Across International (USA). The procedure comprised the following sequential stages: (i) establishment of a deep static vacuum (10^{-3} Pa or 10^{-6} Torr) within a quartz reactor containing a quartz ampoule with a raw material; (ii) introduction of high-purity argon at room temperature to a pressure of 0.3–0.5 bar, calculated to reach 1.1–1.3 bar at the melt temperature of the material (770–800 ° C), in order to suppress the evaporation of aggressive halogen vapors. Crystal growth was conducted in strict accordance with the protocol of the Eurotherm system and the MCGS (Monitor and Control Generated System) human–machine interface (HMI) platform. Owing to this integrated control architecture, a controlled slow-cooling regime of the "superheated" crystal at a rate of 20–30 ° C/h was implemented, a capability not previously attainable in comparable crystal growth systems. The newly developed integrated crystal growth system differs fundamentally from conventional designs and does not require: (i) quartz-sealing laboratory facilities for ampoule sealing, since the raw material within the quartz ampoule is maintained under vacuum inside the quartz reactor; (ii) additional water cooling of the installation, as the crystallization center is formed close to the thermal block and ends of the quartz tube are positioned outside the high-temperature zone. In a test regime, X-ray luminescence (XRL) spectra of freshly grown KCl:Li crystals were recorded as a function of lithium ion concentration. The anticipated enhancement of the luminescence light yield was observed, attributed to the recombination assembly of electron–hole pairs within the field of lithium ions. The result constitutes an important parameter for the development of the scientific basis of scintillation detectors.

Keywords: alkali halide crystal (AHC); single crystal; crystal growth; Bridgman method; X-ray luminescence (XRL); radiation defects; exciton-like luminescence.

Introduction

The results of long-term investigations into the behavior of electronic excitations in alkali halide crystals (AHCs) [1–5] have laid the scientific foundation for the active development of next-generation scintillators, as well as for the optimization of classical scintillation materials intended for application in computed tomography, positron emission tomography, and advanced imaging systems [6–11]. Concurrently, the search for novel dosimetric materials remains ongoing. A representative example is thermoluminescent dosimeters (TLDs) based on LiF single crystals. Owing to the tissue equivalence of LiF with respect to γ-radiation, such TLDs are widely employed in radiobiology, radiation therapy, and biological shielding in neutron environments of nuclear reactors [12–16]. It should be emphasized that the principal dosimetric response is associated with high-temperature peaks of thermally stimulated luminescence (TSL), with maxima at 473 K (TLD-100) and 490 K (TLD-700H) [17–23].

The expanding utilization of advanced materials (cryodetectors and carbon nanotubes of various morphologies [24–29]) further stimulates fundamental research under local [30–32], uniaxial [33–38], and hydrostatic deformation [39–41].

The diversity and scope of such fundamental studies necessitate the availability of well-defined model objects for the targeted search of functional materials. At present, growth of crystals with precisely controlled physical and chemical properties remains a requirement for strategic research directions aimed at enhancing scintillation and dosimetric performance.

We have observed an enhancement of the XRL yield at 2.8 eV and 3.1 eV, which increases with both the Na^+ concentration and the sample temperature, and it is interpreted in terms of the correlated electron–hole (e–h) pairs assembly in the vicinity of Na^+ ions, followed by radiative relaxation proceeding via an exciton-like state [41]. On the basis of the experimentally established XRL enhancement in KCl:Na, we examined [22,41] how feasible this effect may be across the series of alkali-metal chlorides doped with homologous cations smaller than the host-lattice cation. The analysis indicates two key trends. Firstly, the crystal density increases in the following sequence: NaCl (2.1 g/cm^3) $\rightarrow$ KCl (2.2 g/cm^3) $\rightarrow$ RbCl (2.76 g/cm^3) $\rightarrow$ CsCl (3.97 g/cm^3), as well as the effective atomic number (Z_{eff}) KCl (18.1) $\rightarrow$ RbCl (31.2) $\rightarrow$ CsCl (48.3); which provides increasingly favorable conditions for efficient absorption of ionizing radiation energy. Secondly, the ratio of the ionic radius of the host cation to that of the dopant cation increases for Na^+-doped crystals: KCl:Na (1.36) $\rightarrow$ RbCl:Na (1.5) $\rightarrow$ CsCl:Na (1.7); it is expected to create a deeper local potential well, promoting the correlation of e–h pairs.

A number of crystals have been successfully grown using the proposed setup, including KCl:Na and RbCl:Na, with the sodium ion concentration range of 100–1000 ppm. KCl:Li crystals are challenging to grow due to three factors: first, LiCl is superhygroscopic compared to NaCl and requires handling exclusively under an inert gas atmosphere (argon, helium); second, coefficient of lithium's incorporation into the KCl and RbCl matrix is very low ($k_{Li} = 0.02$ [42]) com-

pared to sodium ($k_{\mathrm{Na}} = 0.3$ [42]), complicating the activation (doping) process; and third, the ratio of the radii of potassium and lithium differs significantly: KCl:Li (1.95) or $\left(\frac{r(\mathrm{K}^+)}{r(\mathrm{Li}^+)} = 1.95\right)$. From these considerations, the crystal growth procedures will be demonstrated using KCl:Li as the model crystal.

2. Results and Discussion

2.1. Automated setup for crystal purification and growth

Crystals were purified and grown using a universal experimental crystal growth setup manufactured by Across International (USA) [43].

The setup (Figure 1) differs from conventional systems through the incorporation of modern engineering solutions, both in structural design and in the implementation of the growth process. The system enables the growth of a wide range of single crystals under either an inert gas atmosphere (e.g. N_2, He) after establishing high technical vacuum (10^{-6} Torr): semiconductors (such as Ge, CdTe, ZnSe and InSb), AHCs and rare-earth fluorides (e.g. CaF_2 and BaF_2) for optical and laser applications, scintillation materials (NaI, CsI), dosimetric materials (LiF).

Figure 1. Experimental crystal growth setup implementing the Bridgman method in an argon atmosphere following the establishment of high technical vacuum (10^{-6} Torr).

The central component of the setup is a quartz tube (145 cm in length). Inside the tube, a quartz ampoule containing the raw material for crystal growth is suspended from the upper section (Figure 1). Special flanges equipped with

vacuum-tight seals hermetically close both the upper and lower ends of the quartz tube. In traditional designs, evacuation of the quartz ampoule containing the source material requires preliminary sealing in a quartz-processing laboratory. In traditional designs, evacuation of the quartz ampoule containing the raw material required preliminary sealing in quartz-processing laboratories, while in the present configuration, such procedures are no longer necessary. The substantial distance between the tube ends and the high-temperature zone of the furnace (up to 1200 °C), and high vacuum (10^{-6} Torr), eliminates the need for additional water-cooling of the system [43].

Evacuation of the quartz tube to a pressure of 10^{-6} Torr is achieved using modern oil-free pumping units: a fore-vacuum pump (IDP 7, Agilent) and a turbomolecular pump (KYKY FF 100/300). Vacuum control and monitoring devices ensure stable operation of both pumps, maintaining reliable system performance during extended crystal growth cycles lasting 30–50 h.

The setup is controlled via a digital multi-segment controller of the Eurotherm 3204 series and MCGS HMI [43], which enable programmed regulation of the furnace temperature profile between zones and provide controlled vertical translation at variable speeds throughout the entire technological cycle from gradual heating to operating temperatures, melt homogenization, crystal growth, and final annealing.

Eurotherm 3204 is a digital PID temperature controller, directly connected to thermocouples and heating elements, that executes programmed temperature set points, thereby ensuring stable thermal plateaus, which are critical for defect structure and uniform crystal growth. In Eurotherm, each segment consists of two stages: ramping and dwelling. Ramping corresponds to a controlled variation of temperature at a predefined rate. Physically, this stage governs atomic and ionic diffusion, mobility processes, as well as the formation and relaxation of defects. The dwelling stage, by contrast, maintains the temperature at a fixed set point for a prescribed duration, ensures the completion of phase transformations, and stabilizes the structure prior to the subsequent segment.

Since the set temperature during dwelling does not vary with time, this stage formally represents an isothermal regime. In strict thermodynamic terms, however, it is quasi-isothermal owing to unavoidable fluctuations and external influences. Nevertheless, the average temperature remains constant and no intentional temperature gradient is introduced, as there is no programmed modification of the set point, unlike during ramping. The stability of the dwelling stage depends primarily on the PID parameters (in the present system, the control error does not exceed $\pm 1-2^{\circ}$ C under appropriate tuning), as well as the selected ramp rate, since excessively steep ramping may lead to integral wind-up, resulting in overshoot once the set point is reached.

Another important feature of the Eurotherm programming structure is the possibility of disabling one of the two stages within a segment. For example, during the initial heating stage intended for degassing, moisture removal, etc., a dwelling phase is unnecessary because structural formation has not yet commenced. Conversely, upon entering the operating temperature region, where the thermal field becomes uniform and ionic mobility is activated, the raw material requires a

dwelling period in order to prepare for the upcoming high-temperature phase and ensure subsequent uniformity of crystal growth. In the high-temperature segment corresponding to melt formation and homogenization, both ramping and dwelling stages are essential.

Supervisory control of the operating modes, including real-time acquisition and display of equipment parameters (e.g. translation speed and position), is implemented through the SCADA (Supervisory Control and Data Acquisition) system, an operating environment of which is provided by the MCGS HMI platform [43]. MCGS manages the technological process through operator input of commands and settings, while simultaneously displaying the status of drives, sensors, and alarm conditions.

With a single loading of the charge and without additional sealing of the vacuum system, the installation operates in three sequential modes. First, purification from oxygen-containing impurities (OH, O_2, H_2O, etc.). Second, purification from impurities whose incorporation coefficient k is significantly less than unity ($k \ll 1$), implemented via recrystallization, i.e. zone melting. Third, growth of both undoped and doped crystals with lengths of 5–10 cm. The crystal diameter is determined by the inner diameter of the quartz ampoule and may be selected as 20, 30, 40, or 50 mm.

In their review [42], Gindina et al. provide an exceptionally thorough and rigorous description of the technological principles governing the purification and growth of AHCs, and key approaches outlined therein have been implemented in the present experimental setup, which allows the operator to select the required operating mode in a sequential manner.

Purification from oxygen-containing impurities is achieved by prolonged drying of powdered KCl at 80–85 °C for up to 24 h under high vacuum. For this purpose, identical temperature set points (80–85 °C) are applied to all 3 furnace zones. The turbomolecular pump (KYKY) enables evacuation to a level of 10^{-6} Torr, which is essential for removing residual gases (oxygen, nitrogen, etc.) that could otherwise oxidize the melt or become incorporated into the crystal lattice of the growing sample. An essential condition for effective removal of these impurities is maintaining the KCl temperature below 100 °C. At higher temperatures, oxide formation may occur, thereby hindering purification. Thus, the combination of an appropriate temperature regime and high vacuum promotes maximal removal of oxygen-containing species. A practical indicator of successful purification is the gradual improvement (increase) in the vacuum level.

Prior to crystal growth, preliminary purification is required from not only oxygen-containing, but also from alkaline earth (Ca^{2+}, Sr^{2+}, Ba^{2+}) and multivalent impurities (Al^{3+}, Sm^{3+}, Eu^{3+}, etc.). The most established technique is zone melting, based on the equilibrium distribution of impurities between the melt and the solid phases [42]. Efficient purification of AHCs is achieved when the incorporation coefficient k, defined as the ratio of impurity concentration in the crystal (C_{crystal}) to that in the melt (C_{melt}), differs significantly from unity:

$$k = \frac{C_{\text{crystal}}}{C_{\text{melt}}} < 1. \tag{1}$$

Under this condition, impurities preferentially remain in the molten zone and are progressively displaced along the ingot during recrystallization.

The principle of zone melting consists in translating a molten zone of length l along an ingot of total length L. As the molten region moves, impurities are redistributed in the direction of zone motion. Since $k < 1$, the impurity concentration in the melt exceeds that in the solid phase, resulting in progressive displacement of impurities towards the end of the ingot.

Zone melting is therefore most effective for removing impurities whose coefficient is significantly less than unity. Calculations show that for $k_{\mathrm{Li}} = 0.02$ [42], ten successive zone passes reduce the impurity concentration by approximately three orders of magnitude, whereas an infinite number of passes would theoretically allow purification by up to six orders. For alkaline-earth metals and oxygen-containing impurities in AHCs, the incorporation coefficient typically lies within the range 0.019–0.02 [42]. Consequently, a high degree of purification can be achieved by zone melting, as confirmed by flame photometry measurements. Thus, the recrystallization procedure implemented in the present installation enables the production of AHCs with extremely low concentrations of alkaline-earth and multivalent impurities (to 10^{-2} ppm).

After completion of the removal of oxygen-containing impurities, the furnace is switched to the zone-melting regime. The quartz ampoule containing the raw material is positioned in the upper furnace zone, and an identical temperature exceeding the melting point of the material is set for all three zones (for example, above 770 °C in case of KCl). Once the prescribed temperature is reached, the furnace begins to translate vertically at a slow rate (1–3 mm per hour). As the molten zone traverses the three heating zones, the material within the ampoule alternates between molten and crystalline states, with melting occurring within the heated zones and recrystallization taking place in the inter-zone regions.

However, even under the most favorable conditions, zone melting cannot provide approximately more than one order of magnitude purification from homologous cationic or anionic impurities when k approaches unity. For example, purification of KCl from Rb^+ and Br^- is limited because $k > 0.7$. Therefore, to obtain highly purified AHCs by zone melting, preliminary removal of homologous impurities from the starting material is required. For alkali halide raw materials, containing homologous impurities with segregation coefficients close to unity and lower electron affinity than the host halide, purification in the molten state by treatment with a gaseous halogen corresponding to the host compound is recommended. This approach promotes selective removal of homologous species prior to recrystallization.

After purification from impurities and without breaking the hermetic high-vacuum conditions of the system, the crystal growth stage is initiated. This process consists of the following sequential stages.

1. Establishment of a controlled inert atmosphere.

After disconnection from the pumping system, while maintaining high technical vacuum (10^{-6} Torr) within the quartz reactor, high-purity argon (grade 6.0; 99.9998%) is introduced at room temperature to a pressure of 0.3–0.5 bar to suppress evaporation of the raw material at elevated temperatures. The principal

requirement is that, upon thermal expansion at high temperature, the argon pressure reaches approximately 1.1–1.3 bar, i.e. slightly above atmospheric pressure (> 1.0 bar). Under these conditions, inward air leakage is eliminated, which is essential for stable crystal growth. The internal pressure therefore remains marginally higher than the external pressure, without posing any hazard to the surrounding environment. As a result, the KCl charge within the quartz ampoule is fully immersed in an inert argon atmosphere.

2. Heating the three furnace zones to operating temperatures.

The temperature profile (Table 1, columns 1–2) is designed for the KCl crystalline matrix to minimize equipment operation time and to form an optimal "hot zone" in the central region. By analogy with zone melting, the temperature distribution is defined as follows: Zone I – 800 °C, Zone II – 785 °C, Zone III – 750 °C. The melting point of KCl is 770 °C. With a heating rate of 5 °C/min, the operating regime is reached within approximately 150–160 min (Table 1, column 3). This is followed by a programmed dwelling stage at these temperatures (columns 4–6).

3. Primary dwelling.

This period typically lasts 120–130 min (column 4) and ensures complete homogenization of the melt within the quartz ampoule.

4. Crystal growth stage.

Crystal growth commences once all required parameters are established: translation rate of the quartz ampoule (3 mm/h); direction of movement (upward or downward); duration (1800 min (row 5)). The growth duration must correspond to the programmed dwelling time maintained by the controllers for the three zones.

5. Controlled cooling of the grown crystal.

Cooling is performed at a prescribed rate of 20–30 °C/h by synchronized programming of the three-zone temperature profile. The slow cooling period (approximately 2150 min; row 6) significantly exceeds natural cooling rates and constitutes a critical technological parameter for relieving thermal stresses in the freshly grown crystal. This capability, absent in many conventional crystal growth systems, substantially improves structural integrity and reduces the probability of cracking or defect formation.

Without taking into account the preliminary purification stages, the total duration required for growth of a KCl:Li crystal in a quartz ampoule of 90 mm length exceeds 70.5 h (approximately three days). The single crystals obtained using the above-described technology is presented in Figure 2.

Table 1.
Time map for crystal growth (illustrated for KCl:Li).

No.	Zone temperature (°C)	Time (min)			
		Reaching operating temperature	Homogenization (with correction)	Crystal growth at 3 mm/h (ampoule length is 90 mm)	Synchronization
1	2	3	4	5	6
I	800	160	120	1 800	2 150
II	785	157	123		
III	750	150	130		

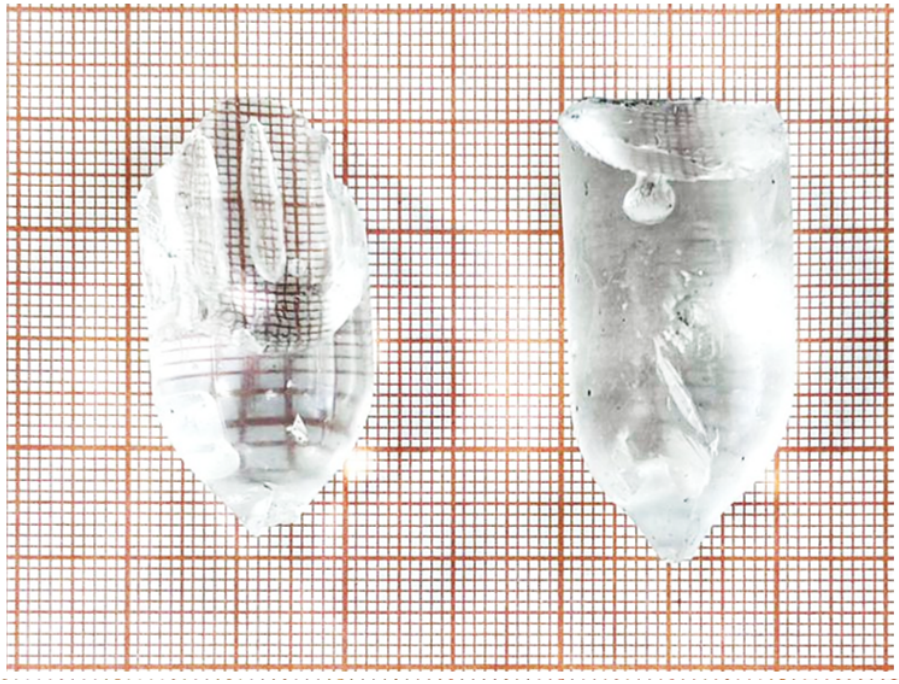

Figure 2. KCl:Li crystals grown by the Bridgman method under static vacuum conditions (10^{-6} Torr) in the reactor, followed by the establishment of an argon atmosphere (1.1–1.3 bar), according to the cyclogram implemented via the HMI.

The KCl:Li crystals were grown from KCl raw material that had been specially purified from oxygen-containing impurities (OH) and homologous anions (Br^-). The charge was prepared by adding LiCl powder that had been preliminary dried under vacuum. Weighing and mixing of the KCl and LiCl powders were performed in a dedicated glove box under an inert atmosphere, since LiCl is highly hygroscopic. The nominal concentration of LiCl introduced into the charge (quartz ampoule containing KCl powder) was 10^4 ppm. Taking into account the lithium incorporation coefficient ($k_{Li} = 0.023$ [42]) in the KCl lattice, the maximum concentration of lithium ions (Li_K^+) in the grown crystal was estimated to be approximately 200 ppm. This maximum value is consistent with flame photometric analysis.

Lithium concentration was determined by flame photometry using a single-channel photometer of model M410 manufactured by Sherwood Scientific (UK) [44]. An optical filter was employed to maximize transmission of the principal lithium resonance emission line at 670.8 nm during combustion of the aerosol generated from a KCl:Li solution. According to absorption spectroscopy measurements, the residual OH concentration was below 0.1 ppm, which corresponds to a three-order-of-magnitude improvement compared with the initial raw material.

In summary, the combined application of high-vacuum (10^{-6} Torr) purification, controlled argon atmosphere processing, and programmed slow cooling (exceeding 35 h) is specifically aimed at obtaining crystals of high chemical purity and structural perfection.

2.1. X-ray luminescence spectra of KCl:Li Crystals

Radiation defects were generated at room temperature under bremsstrahlung X-ray irradiation from an RUP-120 unit equipped with a tungsten anticathode, operated at 3 mA and 100 kV, with a dose exposure of 0.5–1.0 Gy. The registration of XRL, TSL and tunnel luminescence (TL) spectra of the crystals was performed using an MSD-2 high-aperture monochromator coupled with a Hamamatsu H8259-01 photomultiplier operating in photon-counting mode. Spectral scanning in the 6.0–1.5 eV range was carried out using SpectraScan software [45]. XRL spectra were recorded during continuous X-ray irradiation, whereas TL spectra were measured after termination of the ionizing radiation, typically at low temperatures.

It is well established [1, 2] that in nominally pure KCl crystals at low temperatures (4.2 K), the luminescence band at 2.3 eV, attributed to the self-trapped exciton (STE) luminescence, exhibits maximum intensity. With increasing temperature, this emission decreases and vanishes by approximately 40 K.

Within this spectral region, several defect-related emissions are observed in KCl. These include luminescence of excitations localized near single anion vacancies (α-luminescence at 2.6 eV) [2, 46, 47], divacancies (d-luminescence at 3.1 eV) [46, 48], vacancy quartets (q-luminescence at 3.4 eV) [48], as well as F' and VK centers responsible for TL near 3.8 eV [22, 39, 40]. In KCl:Na crystals, luminescence of exciton like formations (ELFs) has also been identified, as they are localized in the field of isolated (2.8 eV) or paired (3.1 eV) sodium impurity ions [35].

In the present work, the XRL spectrum of nominally pure KCl at 300 K reveals very weak, non-elementary emission bands with maxima in the ranges 3.05–3.2 eV and 2.6–2.8 eV (curve 1, Figure 3). The observed broad emission band represents the cumulative contribution of several mutually competing luminescence channels associated with uncontrolled vacancy-type defects [46–48] and residual impurities [45]. It cannot be excluded that even in zone-refined KCl crystals, trace amounts of homologous cations (Li^+, Na^+) persist, giving rise to ELFs in their environment [22, 41, 45].

In the XRL spectrum of KCl:Li doped with a very low lithium concentration (up to 50 ppm), a dominant emission band appears at 2.8 eV. Its intensity exceeds that of nominally pure KCl by more than a factor of 70 (Table 2; compare curves 1 and 2 in Figure 3). With increasing lithium concentration, the intensity of the 2.8 eV band continues to rise systematically. The enhancement relative to pure KCl amounts to 179-fold at 100 ppm, 325-fold at 150 ppm, 433-fold at 200 ppm (curves 2–5 in Figure 3; Table 2).

As the lithium concentration increases, an additional luminescence band emerges with a maximum at 3.16 eV. This band is most likely associated with ELFs localized in the field of paired lithium ions, by analogy with the behavior previously established in KCl:Na crystals [45].

The data presented in Table 2 demonstrate that the crystal growth setup manufactured by Across International enables controlled variation of dopant concentration within a single charge. This capability arises from the implementa-

tion of the zone-melting (recrystallization) regime during growth. The lithium concentration increases progressively along the growth direction, starting from the crystallization center (the point of contact between the conical bottom of the quartz ampoule and the thermal block) towards the upper section of the ampoule (up to 70 mm). Near the crystallization center (bottom of the ampoule), lithium is practically absent (row 1). In the middle section of the crystal, the lithium concentration increases noticeably (rows 2 and 3). In the upper part, it reaches values up to 200 ppm (rows 4 and 5). This behavior is fully consistent with the very low incorporation coefficient of lithium in the KCl lattice.

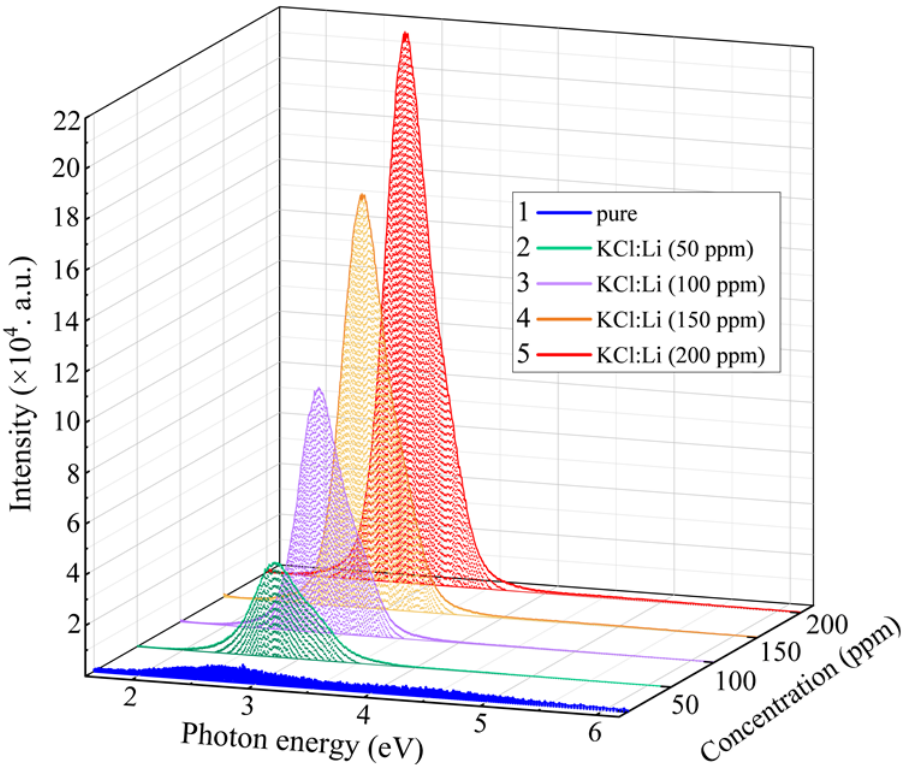

Figure 3. X-ray luminescence spectra at 300 K: 1 – KCl (pure), 2 – KCl:Li (50 ppm), 3 – KCl:Li (100 ppm), 4 – KCl:Li (150 ppm), 5 – KCl:Li (200 ppm).

Table 2.
Dependence of XRL intensity of the KCl crystalline matrix, measured at room temperature, on lithium concentration.

No.	Crystals	Intensity ratio in the region of 2.8 eV ($I_{KCl:Li}/I_{KCl}$)	Intensity ratio in the region of 3.1 eV ($I_{KCl:Li}/I_{KCl}$)
1	KCl (ref.)	1	1
2	KCl:Li (50 ppm)	75	65
3	KCl:Li (100 ppm)	179	141
4	KCl:Li (150 ppm)	325	231
5	KCl:Li (200 ppm)	433	309

It should be emphasized that in KCl:Li (200 ppm) the emission bands at 2.8 eV and 3.1 eV (curve 4, Figure 1) are enhanced by factors of 433 and 309, respectively, relative to nominally pure KCl (curve 1, Figure 3; Table 2).

These experimental results unambiguously demonstrate that the emission bands centered at 2.8 eV and 3.1 eV, whose intensities correlate systematically with increasing lithium concentration in KCl:Li, can with high probability be attributed to ELFs localized in the field of isolated and paired Li^+ ions, respectively. This assignment is supported by the linear growth of the emission intensity at 2.8 eV and 3.1 eV as a function of lithium concentration, a characteristic feature of ELF associated with single (2.8 eV) and paired (3.1 eV) lithium centers.

The integral XRL spectrum of KCl:Li (150 ppm) was decomposed into Gaussian components with maxima at 3.16 eV and 2.8 eV. The corresponding full widths at half maximum (FWHM) are $\Delta_{3.16} = 0.41$ eV and $\Delta_{2.8} = 0.36$ eV (Figure 4). The inset of Figure 4 presents the original fitting data obtained from Gaussian deconvolution, including peak positions, FWHM values, and fitting uncertainties calculated using Origin software.

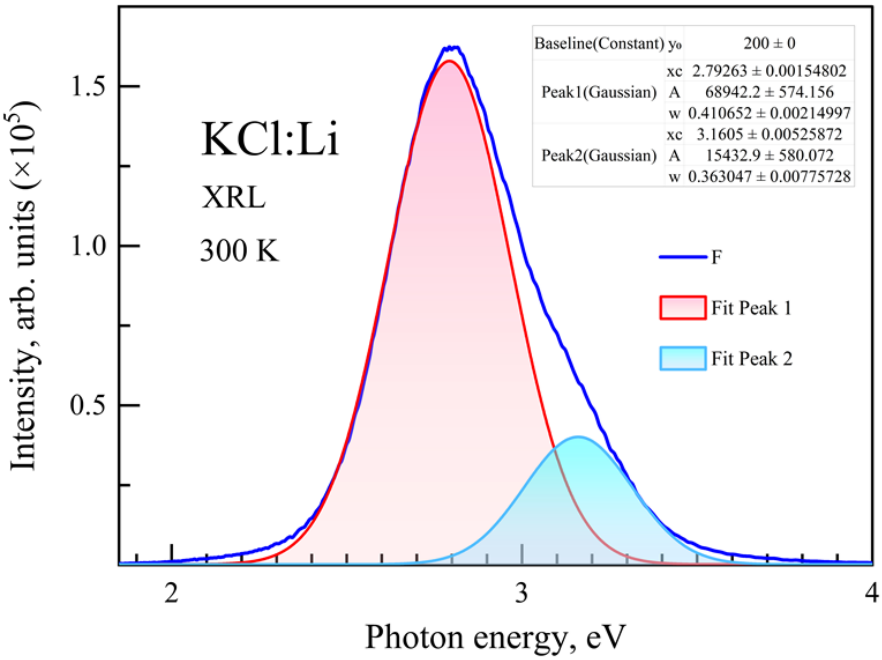

Figure 4. X-ray luminescence spectrum of KCl:Li (150 ppm) at 300 K, resolved into two Gaussian components with maxima at 2.8 eV and 3.1 eV.

Particular attention should be drawn to the intense luminescence bands at 2.8 eV and 3.1 eV observed in KCl:Li crystals (absent in pure KCl), as well as to the continued increase in their intensity with increasing lithium concentration (Figure 3) at room temperature (300 K), where the exciton luminescence at 2.3 eV is thermally quenched.

On the basis of our previous studies [44,45] and the present results, it may be proposed that such intense luminescence at 2.8 eV and 3.1 eV at elevated temperatures (300–400 K) becomes possible due to the assembly of correlated e–h pairs in the electrostatic field of light Li^+ ions. This interpretation, however, requires further experimental verification through selective manipulation of either the electronic or the hole components of ELFs, whose radiative relaxation terminates in the lithium field. For clarity, two types of recombination luminescence may be distinguished depending on the mobile carrier involved: hole–electron recombination luminescence, corresponding to recombination of non-relaxed

holes with localized electrons, and electron–hole recombination luminescence, corresponding to recombination of free electrons with self-trapped holes.

3. Conclusion

On the basis of the experimental crystal growth setup (Across International, USA), a comprehensive technology has been developed for the purification and growth of AHCs, demonstrated using KCl:Li as a representative system. The method enables removal of oxygen-containing, alkaline-earth, and multivalent impurities, followed by crystal growth under conditions of deep technical vacuum (10^{-3} Pa, i.e. 10^{-6} Torr) with the controlled introduction of high-purity argon (grade 6.0; 99.999%) to a pressure of approximately 0.3 bar at room temperature.

The introduction of argon is essential for suppressing evaporation of the melt at elevated temperatures (around 800 °C). Without this measure, halogen vapors may form an aggressive gaseous environment capable of contaminating the entire vacuum system, including oil-free vacuum pumps, potentially leading to equipment failure. In addition, it would result in significant mass loss of the raw material and depletion of isovalent light dopant cations.

A wide range of thermal regimes, controlled by multi-segment Eurotherm 3204 controllers, provides flexible programming of growth cyclograms for both pure and doped crystals using two- or three-zone configurations. Most importantly, a slow-programmed cooling rate of 20–30 °C per hour has been implemented for the first time in this class of systems, ensuring controlled stress relaxation in the grown crystals.

The precision mechanical translation of the quartz ampoule is governed by the SCADA system operating within the MCGS HMI environment throughout the growth cycle.

XRL spectra recorded for freshly grown KCl:Li crystals as a function of lithium concentration revealed a pronounced enhancement of the light yield. This effect, attributed to the recombination assembly of correlated electron–hole pairs in the field of lithium ions, represents a key parameter in the development of the scientific foundations of advanced scintillation detectors.

Acknowledgments

This work was supported by the Science Committee of the Ministry of Science and Higher Education of the Republic of Kazakhstan (Grant No. AP26100001).

References

[1] K.S. Song, R.T. Williams, Self-trapped excitons (Berlin: Springer, 2013) 410 p. [*CrossRef*]
[2] C.B. Lushchik, A.Ch. Lushchik, Decay of electronic excitations with defect formation in solids (Moscow: Nauka) (1989). (In Russian) [*Web Link*]

[3] C. Lushchik, A. Lushchik, Phys. Solid State **60** (2018) 1487–1505. [*CrossRef*]
[4] A. Lushchik, Ch. Lushchik, E. Vasil'Chenko, A.I. Popov, Low Temp. Phys. **44** (2018) 269–277. [*CrossRef*]
[5] E.D. Aluker, D.Yu. Lusis, S.A. Chernov, Electronic excitations and radioluminescence of alkali halide crystals (Riga: Zinatne, 1979) 251 p. (In Russian)
[6] Y. Takizawa et al., J. Cryst. Growth **573** (2021) 126287. [*CrossRef*]
[7] Y. Takizawa et al., Jpn. J. Appl. Phys. **61** (2022) SC1009. [*CrossRef*]
[8] K. Miyazaki et al., Radiat. Phys. Chem. **207** (2023) 110820. [*CrossRef*]
[9] A. Seguchi et al., Opt. Mater. **168** (2025) 117406. [*CrossRef*]
[10] Y. Yoshikawa et al., Radiat. Phys. Chem. **215** (2024) 111367. [*CrossRef*]
[11] H. Kimura et al., J. Lumin. **236** (2021) 118099. [*CrossRef*]
[12] S. Lee, J. Lee, G. Kim, S.J. Ye, Nucl. Instrum. Methods Phys. Res. A **1050** (2023) 168141. [*CrossRef*]
[13] M. Behmadi et al., Nucl. Eng. Technol. **56**(2) (2024) 753–761. [*CrossRef*]
[14] C. Iliaskou et al., Z. Med. Phys. (2025). [*CrossRef*]
[15] E. Saeedian et al., Radioprotection **60**(1) (2025) 57–64. [*CrossRef*]
[16] L. Bossin et al., Radiat. Meas. **188** (2025) 107504. [*CrossRef*]
[17] S. Lee et al., Nucl. Instrum. Methods Phys. Res. A **1050** (2023) 168141. [*CrossRef*]
[18] S.P. Voss et al., Radiat. Meas. **46** (2011) 1590–1594. [*CrossRef*]
[19] A. Romanyukha et al., Radiat. Meas. **108** (2018) 45–51. [*CrossRef*]
[20] E.B. Jumpeno et al., Atom Indones. **50** (2024) 267–271. [*CrossRef*]
[21] M. Alizadeh et al., J. Biomed. Phys. Eng. **12**(2) (2022) 111–116. [*CrossRef*]
[22] N. Salah, P.D. Sahare, A.A. Rupasov, J. Lumin. **124** (2007) 357–364. [*CrossRef*]
[23] Y.S. Horowitz, L. Oster, I. Eliyahu, J. Lumin. **214** (2019) 116527. [*CrossRef*]
[24] H.R. Baghani, M. Goli, E. Koushki, M. Robatjazi, Results Opt. **18** (2025) 100778. [*CrossRef*]
[25] L. Prouzova Prochazkova et al., Radiat. Phys. Chem. **237** (2025) 112991. [*CrossRef*]
[26] Z. Lagha Ameur, P. Lonski, T. Kron, Radiat. Meas. **192** (2026) 107626. [*CrossRef*]
[27] X. Li et al., Nano-Micro Lett. **17**(1) (2025) 160. [*CrossRef*]
[28] P. Mangthong et al., Radiat. Phys. Chem. **237** (2025) 113010. [*CrossRef*]
[29] A.A. Patil et al., Anal. Methods **17**(8) (2025) 1754–1764. [*CrossRef*]
[30] K. Shunkeyev et al., Nucl. Instrum. Methods Phys. Res. B **509** (2021) 7–11. [*CrossRef*]
[31] K. Shunkeyev et al., Nucl. Instrum. Methods Phys. Res. B **509** (2021) 1–6. [*CrossRef*]
[32] K. Shunkeyev et al., J. Lumin. **284** (2025) 121308. [*CrossRef*]
[33] L. Myasnikova et al., Nucl. Instrum. Methods Phys. Res. Sect. B **464** (2020) 95–99. [*CrossRef*]
[34] K. Shunkeyev et al., J. Phys. Conf. Ser. **830** (2017) 012138. [*CrossRef*]
[35] Y. Li, M. Cotlet, I. Hadar, P. Guo, Chem. Commun. **60**(99) (2024) 14806–14809. [*CrossRef*]
[36] Y. Kohzuki, T. Ohgaku, J. Lumin. **253** (2023) 119469. [*CrossRef*]

[37] M. Barth, W. Lorke, E. Mohler, Phys. Status Solidi B **130** (1985) 457–466. [*CrossRef*]
[38] W. Qi et al., Phys. Lett. A **538** (2025) 130351. [*CrossRef*]
[39] S. Mahlik, M. Malinowski, M. Grinberg, Opt. Mater. **33** (2011) 1525–1529. [*CrossRef*]
[40] S. Mahlik, High-pressure study of phosphors emission, in: R.-S. Liu, X. Wang (Eds.), Phosphor Handbook: Experimental Methods for Phosphor Evaluation and Characterization (Boca Raton: CRC Press, 2022) pp. 419–545. [*CrossRef*]
[41] K. Shunkeyev et al., Nucl. Instrum. Methods Phys. Res. B **528** (2022) 20–26. [*CrossRef*]
[42] R. Gindina, A. Maaroos, L. Ploom, N. Jaanson, Development of the method of preparing KCl and KBr crystals containing impurities, in: Electronic excitations and defects in ionic crystals (Tartu: Academy of Sciences of the Estonian SSR, Institute of Physics) (1979) pp. 45–89. (In Russian)
[43] Across International, 1200 °C 3-zone crystal growth tube furnace with Kanthal heating elements, swing open chamber. [*Web Link*]
[44] Sherwood Scientific Ltd., Model 410 flame photometer. [*Web Link*]
[45] K. Shunkeyev et al., Crystals **13**(2) (2023) 364. [*CrossRef*]
[46] C. Lushchik et al., Phys. Status Solidi B **114**(1) (1982) 103–111. [*CrossRef*]
[47] R. Onaka, I. Fujita, A. Fukuda, J. Phys. Soc. Jpn. **18** (1963) 263–268. [*Web Link*]
[48] A.Z. Bekeshev, K.Sh. Shunkeyev, E.A. Vasil'chenko, A.A. Elango, Phys. Solid State **39** (1997) 75–76. [*CrossRef*]